Neoplasia • Vol. 8, No. 7, July 2006, pp. 587–595 587

www.neoplasia.com

Early Effects of Combretastatin A4 Phosphate Assessed by Anatomic and Carbogen-Based Functional Magnetic Resonance Imaging on Rat Bladder Tumors Implanted in Nude Mice[1]

Carole D. Thomas[*,†], *Christine Walczak*[*,†], *Julia Kaffy*[‡,§], *Renée Pontikis*[‡,§], *Jacqueline Jouanneau*[§,¶] *and Andreas Volk*[*,†]

*INSERM, U759, Orsay F-91405, France; [†]Institut Curie Research Center, Orsay F-91405, France; [‡]CNRS, UMR 176, Paris F-75005, France; [§]Institut Curie Research Center, Paris F-75005, France; [¶]CNRS, UMR 144, Paris F-75005, France

Abstract

Combretastatin A4 phosphate (CA4P) causes rapid disruption of the tumor vasculature and is currently being evaluated for antivascular therapy. We describe the initial results obtained with a noninvasive multiparametric magnetic resonance imaging (MRI) approach to assess the early effects of CA4P on rat bladder tumors implanted on nude mice. MRI (4.7 T) comprised a fast spin-echo sequence for growth curve assessment; a multislice multiecho sequence for T_2 measurement before, 15 minutes after, and 24 hours after CA4P (100 mg/kg); and a fast T_{2w}* gradient-echo sequence to assess MR signal modification under carbogen breathing before, 35 minutes after, and 24 hours after CA4P. The tumor fraction with increased T_{2w}* signal intensity under carbogen (T^+) was used to quantify CA4P effect on functional vasculature. CA4P slowed tumor growth over 24 hours and accelerated necrosis development. T^+ decrease was observed already at 35 minutes post-CA4P. Early T_2 increase was observed in regions becoming necrotic at 24 hours post-CA4P, as confirmed by high T_2 and histology. These regions exhibited, under carbogen, a switch from T_{2w}* signal increase before CA4P to a decrease post-CA4P. The combination of carbogen-based functional MRI and T_2 measurement may be useful for the early follow-up of antivascular therapy without the administration of contrast agents.

Neoplasia (2006) **8,** 587–595

Keywords: Rat bladder tumors, mouse, carbogen, fMRI, antivascular therapy.

Introduction

Combretastatin A4 phosphate (CA4P) is a member of a class of low-molecular-weight vascular-disrupting agents (VDAs) that are currently in preclinical and clinical development for antivascular tumor therapy [1,2]. This tubulin-binding drug causes rapid collapse in tumor blood flow *in vivo*, most likely due to disruption of the tubulin cytoskeleton, leading to morphologic changes in endothelial cells. Effects occur rapidly at concentrations well below the maximum tolerated dose and are largely specific to the tumor vasculature. This specificity is currently under investigation, but there is evidence that it correlates with increased vascular permeability—a property of new tumor vessels [3]. A further increase of permeability by CA4P exposure would therefore lead to massive protein leakage, edema, increase in interstitial fluid pressure, and, finally, vascular collapse [1].

The drug has been evaluated on various experimental tumors in rats and mice, with varying results, most likely depending on tumor types and CA4P scheduling and doses. It is currently in phase II clinical trial, and new variants of the drug are under development [4]. From these studies and trials, it turned out that the drug needs to be used in combination with other drugs. It seems to be, indeed, much less efficient on the peripheral tumor vasculature, leaving a viable rim from which the tumor can start growing again.

In this situation (i.e., rapid and heterogeneous response), a precise combination therapy scheduling, which will ideally require noninvasive therapy follow-up by imaging methods with high spatial resolution for safe and frequent measurements, is expected to be mandatory. This holds for preclinical studies on tumor models that are used for the development of combination therapies, as well as for clinical trials and, eventually, clinical routine.

Noninvasive magnetic resonance imaging (MRI) and magnetic resonance spectroscopy (MRS) techniques may become

Address all correspondence to: Carole D. Thomas, U759 INSERM/Institut Curie Research Center Universitaire, Bâtiment 112, Orsay Cedex 91405, France.
E-mail: carole.thomas@curie.u-psud.fr

[1]This work was supported by the Institut Curie (tumor angiogenesis program), the CNRS INSERM interdisciplinary program "Small Animal Imaging," and the "Cancéropôle Ile de France."
Received 10 March 2006; Revised 17 May 2006; Accepted 18 May 2006.

DOI 10.1593/neo.06232

important tools in the performance of this follow-up. Several experimental studies using MRI or MRS techniques have already shown that administration of CA4P can affect a number of MRI/MRS measurable parameters such as transfer constant K^{trans} and initial area under the curve (IAUC), which are provided by dynamic contrast-enhanced (DCE) MRI, apparent water diffusion coefficient (ADC), tumor blood volume, and Pi/NTP [3,5–11].

More precisely, recent studies by DCE-MRI in animals and humans revealed reduction of K^{trans} or IAUC hours after CA4P administration, which is indicative of a rapid decrease of tumor perfusion [5,7,9–11].

Very recently, Thoeny et al. observed, after CA4P treatment, an early decrease of the ADC, followed by an ADC increase, and again a decrease. These findings were attributed to initially nonperfused but viable tumor tissues, appearance of necrosis, and subsequent tumor regrowth [6].

We recently used carbogen-based functional MRI (fMRI) for longitudinal follow-up of a chemically induced hepatocellular carcinoma in mice, and we suggested a new parameter T^+ (the fraction of tumor voxels with increased T_2*-weighted intensity under carbogen) for noninvasive assessment of therapies involving vasculature-targeting drugs [12].

In the current paper, we demonstrate that T^+ is, indeed, modified very early after CA4P administration in a highly vascularized rat bladder tumor model implanted on nude mice. Carbogen-based fMRI was combined with anatomic high-resolution MRI and T_2 measurements leading to a multiparametric MRI protocol for therapy follow-up.

Materials and Methods

Tumor Model

Tumors were grown from NSF14 cells, which are NBTII carcinoma cells stably transfected with fibroblast growth factor-1 (FGF-1 or acidic FGF). NBTII cells were derived from a chemically induced rat bladder carcinoma. These cells do not produce endogenous FGF-1 but possess the FGFR-2b high-affinity FGF-1 receptor on their surface. NSF14 cells are therefore autocrine for this growth factor and are highly tumorigenic after subcutaneous injection into nude mice [13]. The tumors are highly vascularized as a result of FGF-1 production, release of this potent angiogenic growth factor, and paracrine activation of host endothelial cells [14,15]. Consequently, these tumors are expected to be particularly sensitive to CA4P treatment.

NSF14 cells were routinely cultured in Dulbecco's modified Eagle's medium supplemented with 10% fetal bovine serum, 2 mM glutamine, 100 U/ml penicillin, and 100 μg/ml streptomycin (complete medium); no further growth in selective medium was needed. FGF-1 expression and production were maintained over the passages and *in vivo*; the recent use of these autocrine cells was reported by Billottet et al. [15].

Tumors were obtained on the flank after subcutaneous inoculation of 5×10^6 cells/animal. They developed rapidly, and animals were sacrificed within 2 to 3 weeks. Experiments were carried out 6 to 9 days postinduction.

Experiments were performed in accordance with the guidelines for animal experimentation from the Ministère de l'Agriculture et de la Pêche (authorization no. 91-123).

CA4P

CA4 was synthesized following the method reported by Lawrence et al. [16] then converted, as previously described, into its disodium phosphate prodrug, CA4P [17]. Before each experiment, CA4P was dissolved in sterile saline (0.9% NaCl) and given intraperitoneally as single injection at a dose of 100 mg/kg body weight.

MRI

Seven mice were treated with CA4P, and six mice served as controls to determine tumor growth and necrosis without treatment. For MRI experiments, mice were anesthetized with isoflurane (4% for induction; 1.5–2% for maintenance during the entire experiment) and placed in a home-built cradle in supine position. Tubes containing circulating warm water were placed close to the animal to maintain a constant body temperature at 35.7°C (± 0.9°C).

MRI was performed with a 4.7-T Bruker Biospec 47/30 system (BRUKER BioSpin GmbH, Ettlingen, Germany) equipped with actively shielded gradients (200 mT/m) using a homemade slotted cylinder-type radiofrequency probe (d = 44 mm). Respiratory triggering was performed using a highly sensitive home-built pneumatic system, as described previously [18].

The imaging protocol comprised three sequences:

1. A fast spin-echo sequence ("3D RARE") was used for high-resolution screening of the whole tumor and for the measurement of growth curves [field of view (FOV) = $3 \times 3 \times 2.5$ cm^3; matrix dimension = $256 \times 256 \times 50$; RARE factor = 16; and weighted echo time T_{Ew} = 41 milliseconds]. Repetition time (T_R) was determined by actual respiratory frequency, which could be slightly modulated by anesthesia gas concentration, and was kept at around 2 seconds. The acquisition window (2.8 milliseconds) was centered with respect to respiratory motion peaks by means of an adjustable trigger delay (integrated in the external trigger device). This ensured optimal image quality. Tumor volume was measured by manual delineation of tumor borders on each slice of the high-resolution 3D RARE image block.
2. A multislice multiecho (MSME) sequence was used for quantitative T_2 measurements to characterize CA4P effects on this parameter (FOV = 3 cm^2; matrix dimension = 128×128; slice thickness = 1 mm; $T_R \approx$ 2 seconds; $T_{E\ min}$ = 9.6 milliseconds; and equidistant echoes = 8). Parametric T_2 images were calculated by monoexponential fitting (ParaVision; BRUKER BioSpin GmbH). As necrosis was characterized by long T_2 relaxation times in this model, it was determined on T_2 maps by counting the pixels above a T_2 threshold of 93 milliseconds. This threshold was fixed once on an arbitrarily selected T_2 slice containing necrotic regions

in such a manner that the MRI-estimated necrotic fraction matched that determined on the corresponding histologic section (*vide infra*). The percentage of tumor necrosis was then estimated from all slices covering the whole tumor.

3. fMRI was prepared by the optimization of B_0 homogeneity over the tumor using localized shimming (x, y, z) with a one-shot stimulated echo localization sequence (volume-selective stimulated echo protocol; volume dimensions of about 1 cm^3). fMRI was then performed using a fast gradient-echo (GRE) imaging sequence ("GEFI" protocol; FOV = 3 cm^2; slice thickness = 1 mm; T_E = 16.3 milliseconds; T_R = 26.6 milliseconds; and flip angle $\alpha = 30°$), as described in more detail previously [19]. Briefly, 80 sets of 15 slices covering the whole tumor were acquired during the following protocol of breathing gas administration: image sets 1 to 7: reconstituted air (20% O_2/80% N_2); image sets 8 to 10: transition delay air–carbogen; image sets 11 to 48: carbogen (95% O_2/5% CO_2); image sets 49 to 51: transition delay carbogen–air; image sets 52 to 80: reconstituted air. Breathing gas was delivered at 2 l/min through a nosepiece.

fMRI data were processed according to two different protocols: 1) the time course of relative T_{2w}* signal intensity (SI) variation I/I_0 in response to carbogen breathing was recorded in regions of interest (ROI) defined on T_2 maps; 2) images were treated, pixel by pixel, using homemade programs under IDL (Research Systems, Inc., Boulder, CO): difference images were calculated by subtracting mean images ($n = 7$) from the mean image corresponding to the first set. Only significantly different values (Student's t test, $P \leq .05$) were retained for the difference images. They allowed visualization of the spatial distribution of carbogen response. Furthermore, they were used to measure the tumor fractions exhibiting positive [i.e., signal increase (fraction T^+)], negative [i.e., signal decrease (fraction T^-)], or no significant response [(fraction T^0)] to carbogen breathing [12]. These fractions were determined by counting corresponding pixels for all slices covering the whole tumor. ROI for T^+, T^-, and T^0 measurements delimited the whole tumor on each slice. For that, tumor ROI, animal contour, and some anatomic landmarks (spinal cord and vessels) were first carefully defined on high-resolution/high-contrast images from the MSME sequence set. The whole contour pattern was then positioned on the corresponding GRE mean image with the help of anatomic landmarks. Indeed, due to the lower resolution and the lower contrast of the GRE images, this was considered as the most objective procedure of tumor ROI positioning.

fMR images were acquired before, about 35 minutes after, and 24 hours after CA4P injection. Intraperitoneal injection after the control measurement was performed outside the magnet without moving the anesthetized mouse from its cradle. To perform the 35-minute measurement, the cradle was then reinserted into the magnet at the very same position as before.

In addition to tumor measurements, the response to carbogen breathing was systematically monitored in a region comprising the inferior vena cava and the portal vein to verify carbogen arrival into the blood. Indeed, in the presence of carbogen, a signal increase in this region was systematically observed, as described previously [12,19].

Histopathology

Tumors were excised for histopathology directly after the last MRI experiment (i.e., 24 hours after CA4P administration for the treated group). After sacrifice (cervical dislocation), tumors were removed and embedded in OCT (Tissue-Tek, Sakura, Japan), frozen, and serially cut at −20°C in 4-μm-thick slices. Sections were stained with hematoxylin and stained immunochemically for assessment of necrosis, and for qualitative and quantitative descriptions of microvasculature-related characteristics, as described hereafter. Vessels were highlighted by staining the endothelial cells immunochemically for factor VIII (von Willebrand factor) [20]. Staining was carried out using the Dako EnVision kit K4010 (Dako, Trappes, France), with the following protocol: 4-μm-thick sections were fixed in acetone at 4°C (10 minutes). Sections were incubated with peroxidase block for 5 minutes to quench any endogenous peroxidase activity. After washing carefully (5 minutes) with phosphate-buffered saline (PBS) solution, the sections were incubated (30 minutes) with a diluted (1:400) rabbit anti–human von Willebrand factor (polyclonal antibody, code no. A-0082; Dako), which recognizes an endothelial cell surface marker factor VIII, at room temperature. After washing with PBS for 5 minutes, the sections were incubated with peroxidase polymer for 30 minutes. After washing in a PBS solution (5 minutes), the sections were stained by a 10-minute incubation with 3,3′-diaminobenzidine tetrahydrochloride substrate chromogen, which resulted in a brown precipitate at the antigen site (20 μl/ml). Hematoxylin was used for counterstaining. Different incubation steps then dehydrated the sections: 95% alcohol (10 minutes), 100% alcohol (10 minutes, thrice), toluene–alcohol (50/50) mixture (10 minutes), and 100% toluene (10 minutes, twice). Finally, sections were mounted with a cover glass using Eukitt (EMS, Hatfield, PA).

For estimation of tumor necrosis, six adjacent sections located at the tumor center at 200-μm intervals were selected and scanned at 4000 dpi (Nikon Super Coolscan 8000, Tokyo, Japan). The percentage of necrosis was determined by manual delimitation using Amira software (Mercury Computer Systems; TGS, Bordeaux, France).

Apparent microvessel density (MVD) was estimated on immunochemically stained sections in two different rectangular regions, areas 1 and 2 (1.5 × 1.1 mm), characterized by different T_2 evolutions observed on colocalized MRI slices after CA4P administration. MVD estimation was carried out without knowledge of the areas' category. Individual microvessels were counted on digitized images acquired on a Zeiss Axiophot microscope (Carl Zeiss AG, Oberkochen, Germany) equipped with a DXC-990P camera (Sony, Tokyo, Japan) at a final magnification of ×140. Using CAD software (CorelDRAW; Corel Corporation, Ottawa, Canada), a grid was superimposed on the section to facilitate counting. An apparent microvessel was defined as any stained

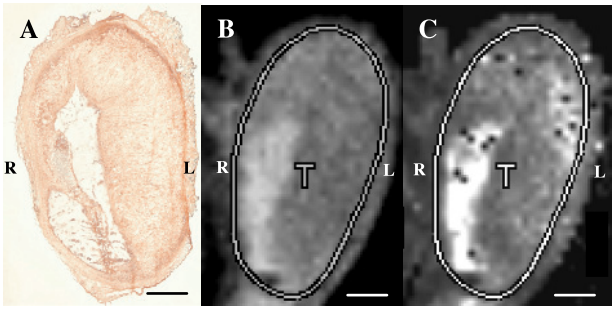

Figure 1. *Comparison of a histologic section (anti–factor VIII staining; scale bar = 1 mm) of a tumor treated by CA4P (A), with corresponding T_2 maps before (B) and 24 hours after CA4P administration (C) (black dots on the post-CA4P T_2 map correspond to pixels with fit failure).*

endothelial cell or cell cluster separated from an adjacent one. Five tumors were inspected.

Statistical Analysis

Correlation of necrotic fractions determined by histology and on T_2 maps was assessed by linear regression analysis ($P < .05$ was considered statistically significant). A comparison of necrotic fractions, tumor growth, MVD values, T^+ values, I/I_0 values, and T_2 values was performed using the Mann-Whitney U test ($P < .05$ was considered statistically significant).

Results

Anatomic MRI and Histology

Control tumors without any treatment were characterized by rapid growth. The mean tumor growth rate was 122 ± 68% per day. Treatment by CA4P considerably slowed growth for all tumors ($n = 5$; two mice died before the second tumor volume determination). The growth rate was 15 ± 24% per day and was statistically different from that of the control group.

Hematoxylin-stained sections revealed that necrosis fraction was significantly higher in the CA4P-treated group (34 ± 18%) than in the control group (12 ± 15%). Furthermore, evolution of necrosis fraction over 24 hours could be studied in both groups through noninvasive estimation by MRI. Indeed, necrotic regions were detected as high T_2 regions in tumors (Figure 1*C*), and necrotic fractions determined by histology (Figure 1*A*) and on T_2 maps were highly correlated [(necHis) = 0.79(necT_2) + 13.1; $r = 0.99$, $P = .003$].

For all treated tumors, we observed a significant increase of necrosis 24 hours after CA4P administration. The necrotic fraction was 25 ± 13% before CA4P administration and was 41 ± 17% afterward. For comparison, in the control group, the percentage of necrosis was 13 ± 9% on the first day and was 18 ± 12% after 24 hours (nonsignificant).

fMRI and Histology

Signal modification on carbogen breathing was observed with the fMRI protocol on all untreated tumors (i.e., control group and treated group pre-CA4P; $n = 13$). However, spatial distribution of carbogen response was heterogeneous, with different time course patterns observed in the same tumor (Figure 2).

CA4P treatment drastically modified carbogen response in the tumors. Typical examples are given in Figures 2 and 3. Figure 2 represents carbogen response in three areas of the same tumor, revealing different response evolutions after CA4P administration: positive response during the carbogen breathing time slot before CA4P treatment and slightly negative response 35 minutes after treatment (Figure 2*A*); no response to carbogen, neither before nor after CA4P treatment (Figure 2*B*); and continuous signal increase on carbogen before CA4P treatment and continuous signal decrease after CA4P treatment (Figure 2*C*). Interestingly, the latter region corresponded to necrosis, as detected on the

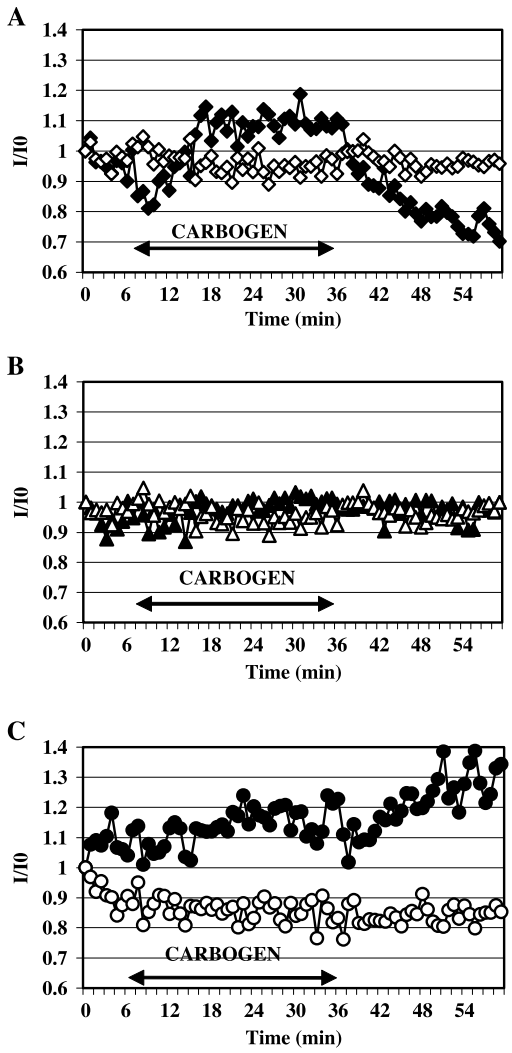

Figure 2. *Time courses of T_{2w}^* signal modification I/I_0 during carbogen breathing before (filled symbols) and 35 minutes after (open symbols) CA4P administration. In a given tumor, three regions could be distinguished by the different effects of CA4P on response to carbogen breathing. (A) Initial T_{2w}^* signal increase on carbogen disappeared post-CA4P. (B) No response to carbogen neither before nor after CA4P treatment. (C) Initial continuous signal increase switched to continuous signal decrease post-CA4P.*

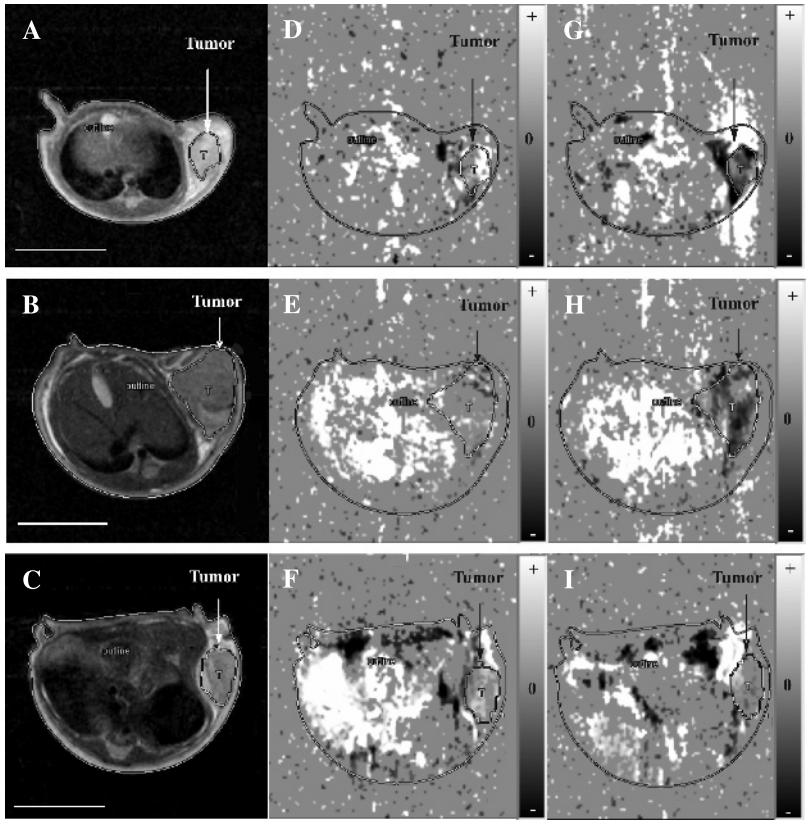

Figure 3. *Visualization of CA4P effect on functional difference images of three tumors (rows). Each row shows a high-resolution T_2-weighted image of a slice passing through the tumor center (A–C) and the corresponding T_{2w}* difference images taken at the center of the carbogen time slot before (D–F) and 35 minutes after (G–I) CA4P administration. The background gray value corresponds to no significant response under carbogen breathing; higher and lower gray values correspond, respectively, to significant positive and negative responses (apparent response outside the animal is due to residual respiratory motion artifacts). After CA4P administration, the disappearance of positively responding regions and the appearance of negatively responding or nonresponding regions are visible in these examples. Scale bar = 1 cm.*

corresponding T_2 map and histologic section (regions are depicted in Figure 6*A*).

Typical images of carbogen response before CA4P treatment and its evolution after treatment are shown on Figure 3. For three tumors, the difference images corresponding to a slice passing through the tumor center and taken in the middle of the carbogen time slot are depicted. The most apparent effect of CA4P treatment seemed to be a decrease of positively responding regions in favor of negatively responding or nonresponding regions (Figure 3, *G*, *H*, and *I*).

Tumor vessel damage caused by CA4P administration was visible on histologic sections. Indeed, immunochemical staining of the vasculature yielded a rather anarchic pattern, which was compatible with important vessel disorganization and vasculature disruption in nonnecrotic areas (Figure 4).

Evolution of the overall response to carbogen was assessed in all treated tumors by measuring fractions with positive (T^+), negative (T^-), and no (T^0) response (*cf.* Materials and Methods section). This procedure was referred to as "functional tumor segmentation."

The pre-CA4P and post-CA4P time courses of these fractions averaged over all tumors are depicted in Figure 5. They showed, at 35 minutes and 24 hours post-CA4P, an important decrease of mean T^+ (Figure 5*A*), as well as an increase of mean T^0 and T^- (Figure 5, *B* and *C*), with a slight nonsignificant trend of recovery toward pre-CA4P values at 24 hours post-CA4P. The highest decrease of mean T^+ was observed between 24 and 36 minutes after carbogen onset [T^+(35 minutes post-CA4P) / T^+(before) = 0.43]. Within this time slot, T^+(35 minutes post-CA4P) was always significantly different from T^+(before); for T^0, the corresponding difference was only significant at the 30-minute measurement; and for T^-, the corresponding difference was not significant. T^+ was therefore considered as the most sensitive parameter evaluating CA4P effect.

As already stated above, T_2 maps were used to estimate tumor necrosis before and 24 hours after CA4P administration. A detailed examination of T_2 maps revealed that T_2 relaxation was already modified in some tumor regions at about 15 minutes post-CA4P. More precisely, after analysis of one axial slice passing through the tumor center, different areas could be distinguished in terms of T_2 variation (Figure 6, *A* and *B*): area 1, where T_2 decreased 15 minutes after CA4P administration and recovered 24 hours after CA4P administration; area 2, where T_2 did not change after CA4P administration; and area 3, where T_2 continually increased after

CA4P administration. Furthermore, after examination of the different corresponding areas on histologic sections stained with factor VIII (Figure 6*A*), we observed, for all tumors, that area 1 had higher apparent MVD (651 vessels/mm^2 ± 102) than area 2 (296 vessels/mm^2 ± 40, P = .001), and that area 3 corresponded to necrotic and "prenecrotic" regions. Qualitatively, compared to area 2, in area 1, the vessel lumen was more visible and the network architecture seemed to be more anarchic with more vessel ramifications.

In addition, I/I_0 ratios were measured in these areas during the central time slot shown in Figure 5. The results are depicted in Figure 6*C*. In area 1, I/I_0 decreased significantly at 35 minutes after CA4P administration, but no further significant decrease at 24 hours was observed. In area 2, I/I_0 was not modified by CA4P; in area 3, the necrotic area was characterized by an important decrease of I/I_0 at 35 minutes after CA4P, which was even more pronounced at 24 hours.

Discussion

In the present study, the early effect of the administration of a unique CA4P dose to nude mice bearing subcutaneously grown hypervascular rat bladder tumors was assessed by completely noninvasive MRI approaches and by histology. The effects of CA4P on tumor growth, necrosis, and functional vasculature were demonstrated by comparing a nontreated control group with the treated group, and, more importantly, by performing a 24-hour longitudinal follow-up of CA4P administration on the treated group.

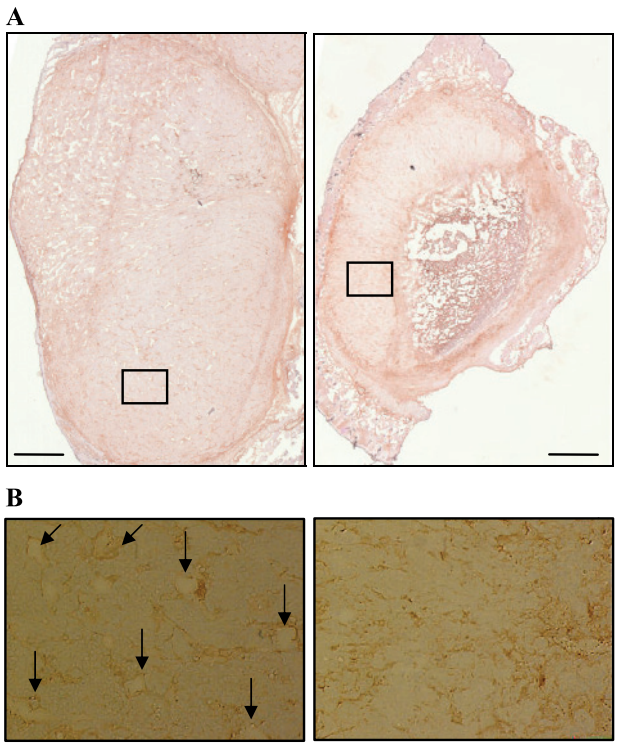

Figure 4. *Histologic sections stained with hematoxylin and antibody anti–factor VIII (slice thickness = 4 μm) of (A; left) a control tumor and (A; right) a treated tumor (scale bar = 1 mm). (B) Comparison of the rectangular regions at higher magnification (×20) reveals vessel damage caused by CA4P administration in the treated tumor. Arrows indicate distinct vessels with lumen on the control tumor section, which are hardly visible on the treated tumor section.*

Tumor Growth and Morphology

We observed that rat bladder's tumor growth rate was considerably slowed by a unique dose of CA4P at 100 mg/kg. Our results are in accordance with those of Ahmed et al. [21], which were obtained on R1 rat rhabdomyosarcoma, but differed from those of Chaplin and Hill [22], who observed nonsignificant growth retardation on murine tumors (CaNT). The discrepancy with respect to the latter study might be explained by the tumor model used in our study, which should contain a high fraction of permeable neovessels due to an overproduction of FGF-1. This property is likely to sensitize the tumor to VDAs [1].

The longitudinal follow-up of necrosis on T_2 maps confirmed the tumor structure modification and destruction induced by CA4P in our model. Indeed, we observed a 62% increase of necrosis fraction at 24 hours posttreatment, compared to a 41% increase over 24 hours in the control group. Furthermore, modifications of vascular aspects, namely, important vessel disorganization and vasculature disruption, were observed in nonnecrotic areas on factor VIII–stained histologic sections.

Functional Vasculature

The effect of CA4P on functional tumor vasculature was evaluated by carbogen-based fMRI, using our recently introduced approach for functional segmentation, where we quantify tumor fractions with positive, negative, or no response after about 30 minutes of carbogen breathing.

From the results depicted in Figure 5, we concluded that T^+ should be the most sensitive parameter to follow CA4P effect. In our experiments, the first post-CA4P fMRI measurement was performed about half an hour after drug administration. This was the earliest possible time point compatible with our experimental MRI protocol. At this moment, a significant T^+ decrease was observed, which is compatible with an acute decrease in tumor perfusion consequent to vascular destruction. Indeed, other groups, using various methods [positron emission tomography (PET), DCE-MRI, and autoradiography], also described a very early decrease in tumor perfusion in various human and experimental tumors following CA4P administration [10,23–25]. Tozer et al. [26], using intravital microscopy, showed that a complete tumor blood flow shutdown can be obtained within 20 minutes after VDA administration. Zhao et al. [27] found a significant decrease in perfusion/permeability at 2 hours following CA4P administration. In addition, in a recent phase I clinical trial, Anderson et al. [23] showed significant reductions in tumor perfusion, as measured with PET 30 minutes after CA4P administration. A very rapid response was described by Hori et al. [28] using the hydrogen clearance method with a CA4P derivative (AC7700). They observed, using intravital microscopy, that tumor blood flow began to decrease immediately after drug administration and reached a minimum at approximately 30 minutes after injection. All

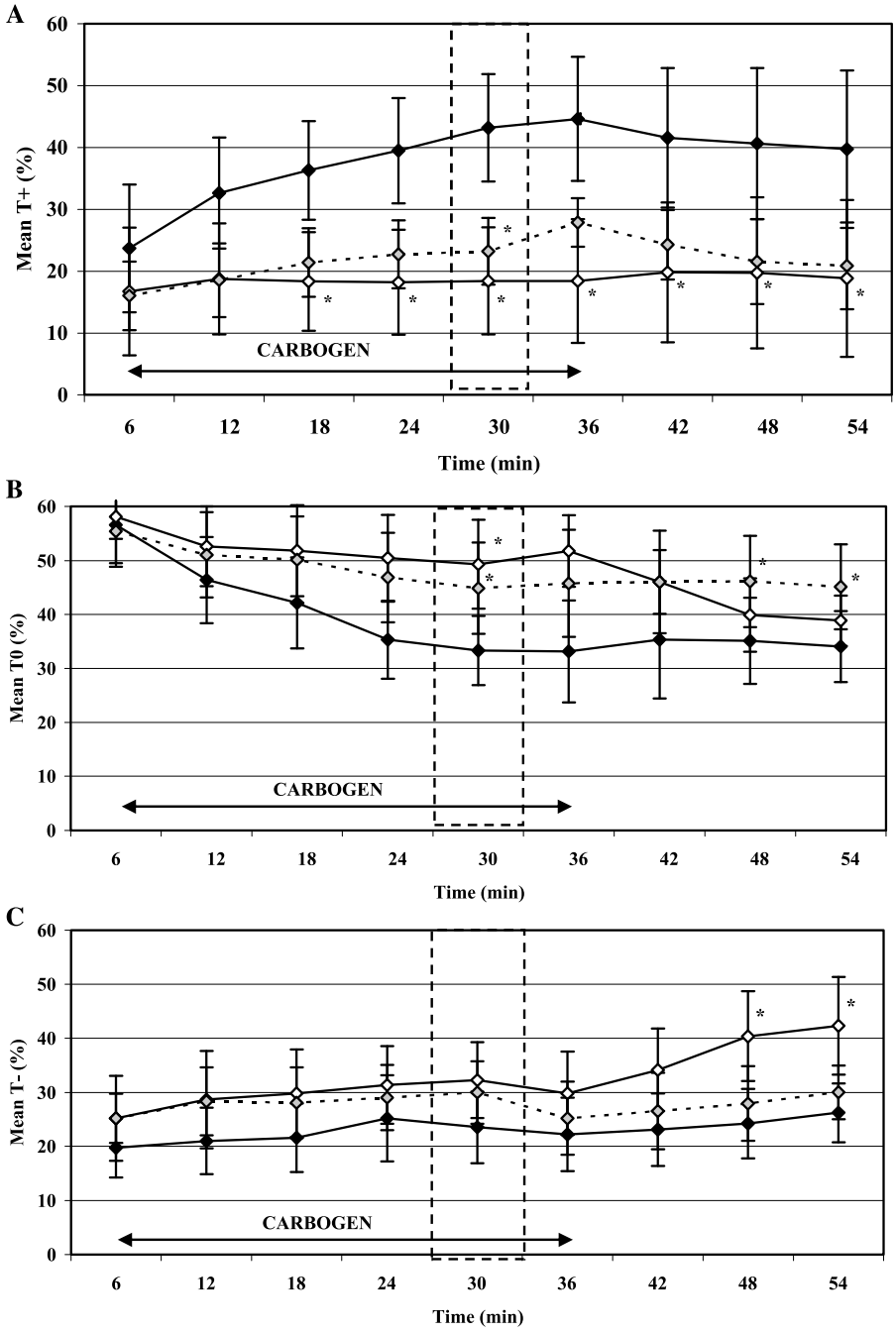

Figure 5. *Evolution of (A) mean T^+ fractions, (B) mean T^0 fractions, and (C) mean T^- fractions during carbogen breathing before (black rhombi), about 35 minutes after (open rhombi), and 24 hours after (gray rhombi) CA4P administration (asterisks indicate statistical differences). Dotted boxes indicate the time window for T_{2w}* signal measurements during longitudinal follow-up (cf. Figures 3 and 6).*

these observations are, indeed, consistent with known pharmacokinetic data of CA4P. CA4P is rapidly dephosphorylated by nonspecific endogenous phosphatases that are present in plasma and on endothelial cells to the active CA4 with a half-life of a few minutes [8].

In our study, the mean T^+ measured at 24 hours was similar to the value at 35 minutes post-CA4P, indicating the persistence of CA4P effect on the tumor vasculature for this tumor model, which may also provide an explanation for a nearly arrested tumor growth. However, an apparent trend of reincrease of T^+ at 24 hours may indicate the start of a progressive recovery of the functional vasculature that is prone to triggering tumor regrowth, as described by others [5].

Interestingly, an early effect of CA4P was not only observed on carbogen-based fMRI but also on parametric T_2 maps without carbogen breathing. In fact, in all tumors, we identified regions characterized, at 15 minutes post-CA4P, by either T_2 decrease (area 1), unchanged T_2 (area 2), or T_2 increase (area 3). We will discuss this observation in more detail (Figure 6). I/I_0 modification under carbogen measured in the same regions revealed a switch from signal increase to no modification, no modification before and after CA4P,

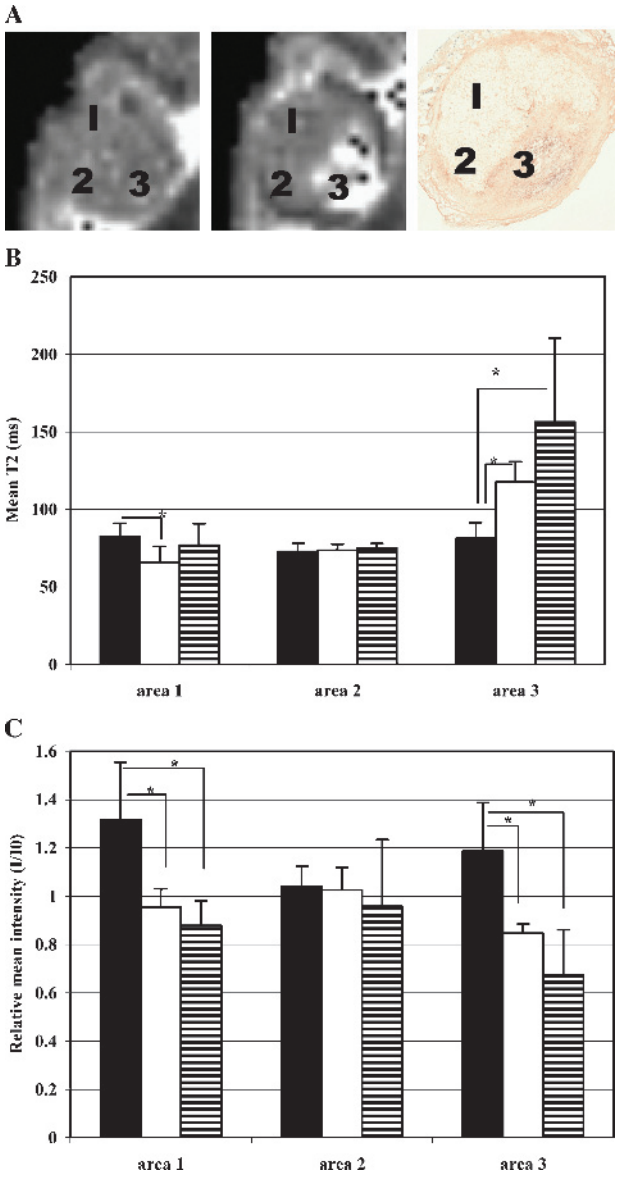

Figure 6. *Regional modifications of T_2 and I/I_0 (T_{2w}* SI variation) after CA4P administration in three different tumor areas. (A) Representative example of location of three areas (labeled 1, 2, and 3) chosen on a central slice of a given tumor. From left to right: T_2 map before and 24 hours after CA4P administration; corresponding histologic section stained with hematoxylin and antibody anti–factor VIII. (B) Mean T_2 values from areas defined on central slices of all treated tumors, measured before treatment (black; n = 6), 15 minutes post-CA4P (white; n = 6), and 24 hours post-CA4P (dashed; n = 5). (C) Corresponding mean I/I_0 measured on the time slot shown in Figure 5 (asterisks indicate statistical differences).*

and from signal increase to signal decrease. The behavior of the latter region, obviously the most sensitive to CA4P, might be explained by rapid edema formation [1] (higher T_2) and a "steal effect" [19,29] during carbogen breathing (T_{2w}* SI decrease). CA4P treatment should indeed create such tumor regions with definitely nonfunctional vasculature, which may generate or enhance such a steal effect. This region was necrotic at 24 hours (histology) and was characterized by even higher T_2, and, more importantly, T_{2w}* SI decrease.

CA4P administration had apparently no effect on MRI parameters measured in area 2. MVD estimation on factor VIII–stained histologic sections provided a much lower value in this region (about 300 vessels/mm^2) compared to area 1 (about 650 vessels/mm^2). From the current study, we cannot decide whether functional MVD in this region was too low to produce a carbogen effect, or, on the contrary, whether the region was well oxygenated through a mature and robust vasculature, which would also be less sensitive to CA4P.

The early T_2 decrease (area 1) might be due to an increase of deoxyhemoglobin as a consequence of vascular disruption, which should be also responsible for the disappearance of carbogen response in this region at 35 minutes post-CA4P. However, with this hypothesis, damage would be less severe than in area 3, as T_2 recovered at 24 hours and the region was not necrotic.

These results also demonstrate the spatial heterogeneity of CA4P effect in our tumor model. Some authors who used the contrast-enhancing agent GdDTPA on mouse and human tumors models also observed an important response heterogeneity to CA4P [3]. They hypothesized, based on the study of Furman-Haran et al. [30], that this heterogeneity may be explained by the angiogenic "hot spots" that exist around necrotic regions of tumors and indicate a heterogeneous distribution of growth factors. For this group, the vascular disruption caused by CA4P results more in the loss of perfusion in specific tumor regions, rather than in the reduction of the overall rate of perfusion in the tumor. However, Maxwell et al. [10], assessing the CA4P antivascular effect by DCE-MRI in rats bearing P22 carcinosarcomas, did not observe any significant tumor heterogeneity.

Further studies, including histology at 35 minutes post-CA4P or DCE-MRI, will be necessary to better understand vascular and cellular modifications that produce the early effects on T_2 and T_{2w}* SI.

In conclusion, the present experimental work at 4.7 T demonstrated, for the first time, that completely noninvasive fMRI based on carbogen breathing provides a new parameter (the tumor fraction T^+) that is useful for monitoring the early effects of antivascular drugs in tumors. Modifications of T_{2w}* SI under carbogen were detected in some tumor regions at about half an hour after CA4P administration. In addition, our results suggest that a CA4P effect can be detected early even by classic T_2 mapping without carbogen breathing, and a combination of both parameters may better assess the sensitivity of the tumor to CA4P treatment. The predictive value of the observed early modifications for therapy outcome will have to be further studied. Carbogen-based fMRI, alone or in combination with T_2 mapping, may become a tool for noninvasive follow-up of therapies involving VDAs, using MRI sequences routinely available on clinical systems and avoiding the administration of exogenous contrast agents.

References

[1] Tozer GM, Kanthou C, and Baguley BC (2005). Disrupting tumour blood vessels. *Nat Rev* **5,** 423–435.
[2] West CM and Price P (2004). Combretastatin A4 phosphate. *Anticancer Drugs* **15,** 179–187.
[3] Beauregard DA, Hill SA, Chaplin DJ, and Brindle KM (2001). The

susceptibility of tumors to the antivascular drug combretastatin A4 phosphate correlates with vascular permeability. *Cancer Res* **61,** 6811–6815.

[4] Hori K, Saito S, and Sato Y (2003). Differential relationship between changes in tumour size and microcirculatory functions induced by therapy with an antivascular drug and with cytotoxic drugs: implications for the evaluation of therapeutic efficacy of AC7700 (AVE8062). *Eur J Cancer* **39,** 1957–1966.

[5] Stevenson JP, Rosen M, and Sun WJ (2003). Phase I trial of the antivascular agent combretastatin A4 phosphate on a 5-day schedule to patients with cancer: magnetic resonance imaging evidence for altered tumor blood flow. *J Clin Oncol* **21,** 4428–4438.

[6] Thoeny HC, De Keyzer F, Vandecaveye V, Chen F, Sun X, Bosmans H, Hermans R, Verbeken EK, Boesch C, Marchal G, et al. (2005). Effect of vascular targeting agent in rat tumor model: dynamic contrast-enhanced *versus* diffusion-weighted MR imaging. *Radiology* **237,** 492–499.

[7] Bentzen L, Vestergaard-Poulsen P, and Nielsen T (2005). Intravascular contrast agent–enhanced MRI measuring contrast clearance and tumor blood volume and the effects of vascular modifiers in an experimental tumor. *Int J Radiat Oncol Biol Phys* **61,** 1208–1215.

[8] Dowlati A, Robertson K, Cooney M, Petros WP, Stratford M, Jesberger J, Rafie N, Overmoyer B, Makkar V, Stambler B, et al. (2002). A phase I pharmacokinetic and translational study of the novel vascular targeting agent combretastatin A-4 phosphate on a single-dose intravenous schedule in patients with advanced cancer. *Cancer Res* **62,** 3408–3416.

[9] Galbraith SM, Maxwell RJ, and Lodge MA (2003). Combretastatin A4 phosphate has tumor antivascular activity in rat and man as demonstrated by dynamic magnetic resonance imaging. *J Clin Oncol* **21,** 2831–2842.

[10] Maxwell RJ, Wilson J, Prise VE, Vojnovic B, Rustin GJ, Lodge MA, and Tozer GM (2002). Evaluation of the anti-vascular effects of combretastatin in rodent tumours by dynamic contrast enhanced MRI. *NMR Biomed* **15,** 89–98.

[11] Zhao D, Jiang L, Hahn WH, and Mason RP (2005). Tumor physiologic response to combretastatin A4 phosphate assessed by MRI. *Int J Radiat Oncol Biol Phys* **62,** 872–880.

[12] Thomas CD, Chenu E, Walczak C, Plessis MJ, Perin F, and Volk A (2004). Relationship between tumour growth rate and carbogen-based functional MRI for a chemically induced HCC in mice. *Magma* **17,** 271–280.

[13] Jouanneau J, Gavrilovic J, Caruelle D, Jaye M, Moens G, Caruelle JP, and Thiery JP (1991). Secreted and non secreted forms of αFGF produced by transfect epithelial cells are active on cell morphology, motility and invasive potential. *Proc Natl Acad Sci USA* **88,** 2893–2898.

[14] Jouanneau J, Plouet J, Moens G, and Thiery JP (1997). FGF-2 and FGF-1 expressed in rat bladder carcinoma cells have similar angiogenic potential but different tumorigenic properties *in vivo*. *Oncogene* **14,** 671–676.

[15] Billottet C, Janji B, Thiery JP, and Jouanneau J (2002). Rapid tumor development and potent vascularization are independent events in carcinoma producing FGF-1 or FGF-2. *Oncogene* **21,** 8128–8139.

[16] Lawrence NJ, Ghani FA, Hepworth LA, McGown AT, and Pritchard RG (1999). The synthesis of (*E*) and (*Z*)-combretastatins A-4 and phenanthrene from *Combretum caffrum*. *Synthesis* **9,** 1656–1660.

[17] Pettit GR and Rhodes MR (1998). Antineoplastic agents 389. New syntheses of the combretastatin A-4 prodrug. *Anti-Cancer Drug Des* **13,** 183–191.

[18] Cohen-Solal C, Parquet M, Tiffon B, Volk A, Laurent M, and Lutton C (1995). Magnetic resonance imaging for the visualization of cholesterol gallstones in hamster fed a new high sucrose lithogenic diet. *J Hepatol* **22,** 486–494.

[19] Thomas CD, Chenu E, Walczak C, Plessis MJ, Perin F, and Volk A (2003). Morphological and carbogen-based functional MRI of a chemically induced liver tumor in mice. *Magn Reson Med* **50,** 522–540.

[20] Yamamoto A, Dhar DK, El-Assal ON, Igarashi M, Tabara H, and Nagasue N (1998). Thymidine phosphorylase (platelet-derived endothelial cell growth factor), microvessel density and clinical outcome in hepatocellular carcinoma. *J Hepatol* **29,** 290–299.

[21] Ahmed B, Van Eijk LI, Bouma-ter Steege JCA, Van der Schaft DWJ, Van Esch A, Joosten-Achjanie SR, Lambin P, Landuyt W, and Griffioen AW (2003). Vascular targeting effect of combretastatin A-4 phosphate dominates the inherent angiogenesis inhibitory activity. *Int J Cancer* **105,** 20–25.

[22] Chaplin DJ and Hill SA (2002). The development of combretastatin A4 phosphate as a vascular targeting agent. *Int J Radiat Oncol Biol Phys* **54,** 1491–1496.

[23] Anderson HL, Yap JT, Miller M, Robbins A, Jones T, and Price PM (2003). Assessment of pharmacodynamic vascular response in a phase I trial of combretastatin phosphate. *J Clin Oncol* **21,** 2823–2830.

[24] Rustin GJS, Galbraith SM, Anderson H, Stratford M, Folkes LK, Sena L, and Price PM (2003). Phase I clinical trial of weekly combretastatin A4 phosphate: clinical and pharmacokinetic results. *J Clin Oncol* **21,** 2815–2822.

[25] Tozer GM, Prise VE, Wilson J, Locke RJ, Vojnovic B, Stratford M, Dennis MF, and Chaplin DJ (1999). Combretastatin A-4 phosphate as a tumor vascular-targeting agent: early effects in tumors and normal tissues. *Cancer Res* **59,** 1626–1634.

[26] Tozer GM, Prise VE, Wilson J, Cemazar M, Shan S, Dewhirst MW, Barber PR, Vojnovic B, and Chaplin DJ (2001). Mechanisms associated with tumor vascular shut-down induced by combretastatin A-4 phosphate: intravital microscopy and measurement of vascular permeability. *Cancer Res* **61,** 6413–6422.

[27] Zhao D, Jiang L, Hahn WH, and Mason RP (2005). Tumor physiologic response to combretastatin A4 phosphate assessed by MRI. *Int J Radiat Oncol Biol Phys* **62,** 872–880.

[28] Hori K, Saito S, and Kubota K (2002). A novel combretastatin A-4 derivative, AC7700, strongly stanches tumour blood flow and inhibits growth of tumours developing in various tissues and organs. *Br J Cancer* **86,** 1604–1614.

[29] Robinson SP, Rodrigues LM, Ojugo AS, McSheehy PM, Howe FA, and Griffiths JR (1997). The response to carbogen breathing in experimental tumor models monitored by gradient-recalled echo magnetic resonance imaging. *Br J Cancer* **75,** 1000–1006.

[30] Furman-Haran E, Margalit R, Grobgeld D, and Degani H (1996). Dynamic contrast-enhanced magnetic resonance imaging reveals stress-induced angiogenesis in MCF7 human breast tumors. *PNAS* **93,** 6247–6251.